APL Materials

Sensing of explosive vapor by hybrid perovskites: Effect of dimensionality

Cite as: APL Mater. **8**, 071106 (2020); https://doi.org/10.1063/5.0011229
Submitted: 19 April 2020 . Accepted: 12 June 2020 . Published Online: 10 July 2020

J. R. Harwell, J. M. E. Glackin, N. J. L. K. Davis, R. N. Gillanders, D. Credgington, G. A. Turnbull, and I. D. W. Samuel

Sensing of explosive vapor by hybrid perovskites: Effect of dimensionality

Cite as: APL Mater. 8, 071106 (2020); doi: 10.1063/5.0011229
Submitted: 19 April 2020 • Accepted: 12 June 2020 •
Published Online: 10 July 2020

J. R. Harwell,[1] J. M. E. Glackin,[1] N. J. L. K. Davis,[2] R. N. Gillanders,[1] D. Credgington,[3] G. A. Turnbull,[1,a)] and I. D. W. Samuel[1,a)]

AFFILIATIONS

[1]Organic Semiconductor Centre, SUPA, School of Physics and Astronomy, University of St Andrews, St Andrews KY16 9SS, United Kingdom
[2]School of Chemical and Physical Sciences, Victoria University of Wellington, Wellington 6140, New Zealand
[3]Cavendish Laboratory, J.J. Thomson Ave., Cambridge CB3 0HE, United Kingdom

[a)]**Authors to whom correspondence should be addressed:** gat@st-andrews.ac.uk and idws@st-andrews.ac.uk

ABSTRACT

Lead halide perovskites are very promising materials for many optoelectronic devices. They are low cost, photostable, and strongly photoluminescent materials, but so far have been little studied for sensing. In this article, we explore hybrid perovskites as sensors for explosive vapor. We tune the dimensionality of perovskite films in order to modify their exciton binding energy and film morphology and explore the effect on sensing response. We find that tuning from the 3D to the 0D regime increases the PL quenching response of perovskite films to the vapor of dinitrotoluene (DNT)—a molecule commonly found in landmines. We find that films of 0D perovskite nanocrystals work as sensitive and stable sensors, with strong PL responses to DNT molecules at concentrations in the parts per billion range. The PL quenching response can easily be reversed, making the sensors reusable. We compare the response to several explosive vapors and find that the response is strongest for DNT. These results show that hybrid perovskites have great potential for vapor sensing applications.

INTRODUCTION

Detecting explosives via the vapors they emit is important for military, law enforcement and humanitarian agencies for detecting landmines, improvised explosive devices, and unexploded ordnance. Sensitive detection of explosives in vapor form is of crucial importance to global counter-terrorism and demining efforts to detect trace signatures of concealed explosive devices. Currently, trained sniffer dogs offer the "gold standard" in explosive vapor detection, being able to detect parts per trillion to parts per quadrillion concentrations of explosive.[1] However, they can only work for short periods before becoming fatigued, and their accuracy and reliability are strongly dependent on the level of training received by both the dogs and their handlers. There are also many conditions where sniffer dogs are unable to operate, such as areas with high heat and humidity. It has therefore been a goal for many years to be able to replicate the sensitivity of sniffer dogs in an electronic nose to produce a device that does not require such extensive training for both sensor and operator, and works consistently each time, no matter what the local conditions.

Such an "electronic nose" requires materials with properties that measurably change when exposed to very low levels of explosive vapors. Organic semiconductors have shown promising results in this area since their sensitivity to nitroaromatics via fluorescence quenching was first demonstrated in the late 1990s by Swager *et al.*[2–6] In this case, quenching is caused by the offset between the lowest unoccupied molecular orbital (LUMO) of the polymer and the explosive vapor, which leads to rapid electron transfer to the explosive and quenching of the polymer fluorescence. Their sensitivity combined with a relatively simple fabrication of sensors via solution processing and easy-to-measure optical response has made them ideal candidates for the next generation of explosive sensors.[7]

This technology has been developed in the FIDO system[8] deployed by the US military, and other field-deployable prototype systems by Arbense[9] and Gillanders *et al.*[10] have been developed, showing promising results.

In recent years, halide perovskites based on the ABX_3 crystal structure (henceforth referred to as "perovskites") have emerged as promising new semiconductor materials with excellent performance both as light absorbers in solar cells[11] and as emitters in light-emitting diodes (LEDs).[12] In addition to good performance in optoelectronic devices, these materials make very attractive candidates as sensing materials due to their strong photoluminescence (PL), resistance to photooxidation,[13] and extremely low-cost starting materials. For instance, the low dark current and high mobility-lifetime product of $CH_3NH_3PbI_3$ photodetectors has attracted a lot of interest as x-ray detectors for advanced medical applications,[14] while perovskite microstrips have been used as highly effective humidity sensors due to the strong and reversible dependence of their conductivity on humidity.[15] Arrays of perovskite photodiodes are now also seeing increased use for image sensors, which have considerable advantages over normal silicon photodiodes because they are blind to thermal noise from the near-infrared part of the spectrum.[16,17]

In addition to their photovoltaic properties, the light emission from perovskites can also be exploited to make novel sensors. Fang *et al.* recently showed that the PL of $CH_3NH_3PbBr_3$ single crystals can be enhanced by up to two orders of magnitude by the addition of oxygen to its otherwise pure nitrogen environment.[18] Recent reports have also shown that fluorescence quenching of $CH_3NH_3PbBr_3$ can be used to detect certain materials in the gas or solution phase, such as the work of Ruan *et al.*, who detected ammonia by observing the reversible reaction of the gas with the film to make a non-perovskite phase, thus quenching the PL until the reaction was reversed by desorption of the ammonia.[19] Single crystals of 1D perovskites have also been used by Zhu *et al.*, who showed that Fe^{3+} ions in a dimethylformamide solution can strongly inhibit radiative recombination by capturing electrons from the perovskite, thus producing a highly sensitive and selective ion detector.[20] Finally, Muthu *et al.* showed that nanocrystals of $CH_3NH_3PbBr_3$ are sensitive to the presence of picric acid in solution, showing their potential for explosive sensing.[21] However, they observed only a very slow response to the picric acid in vapor form and were not able to achieve good sensing of contemporary military explosives such as 2,4,6-trinitrotoluene [$C_7H_5(NO_2)_3$] (TNT), indicating that more work is required to develop hybrid perovskite explosive vapor sensors.

Here, we explore the potential for hybrid perovskites to make effective, low-cost, and reusable sensors for explosive vapors. Two potential challenges with perovskite materials are that they may offer poor permeability to explosive vapors due to their crystalline nature, and many of their defect sites for non-radiative recombination exist at the crystal surfaces. These may limit the ability for a target analyte molecule to cause significant PL quenching, due to limited surface area for interaction that already has a high density of quenching sites, meaning that the addition of further quenching analytes on the surface may not make a major difference to the PL intensity. In order to unlock the potential of perovskites as efficient and low-cost explosive sensors, we aimed to overcome these challenges by tuning the dimensionality of the perovskite unit cell. Tuning the dimensionality will strongly alter the morphology of the perovskite films, while also changing the exciton binding energy and nature of the recombination mechanisms so could potentially enable explosive analytes to have a larger effect.

For applications in solar cells, the most commonly used perovskite has a 3D crystalline structure, which enables strong absorption and easy movement of charge, but also results in a dense structure with a high concentration of charge trapping sites, generally concentrated at crystal boundaries. These films therefore tend to have low photoluminescence quantum yields (PLQY), except at high excitation densities where radiative bimolecular recombination occurs before charges can diffuse to trap sites at the crystal boundaries. In order to make efficient light-emitting devices, the perovskite community has since developed lower-dimensional forms of perovskites such as quasi-2D Ruddlesden–Popper phases,[22,23] 1D perovskite nanowires,[24] and 0D perovskite nanocrystals (PNCs).[25] The increased quantum confinement introduced by the insulating layers in these materials has been shown to increase the exciton binding energy to hundreds of meV,[26] such that photoexcitation leads to the generation of bound excitons, which are funneled into the lowest bandgap region, where they can emit light with high efficiency. These interesting properties have enabled perovskite LEDs to go from efficiencies of less than 1% in 2014[27] to more than 20% in 2020.[28] Other groups have tuned the perovskite dimensionality even further by producing zero-dimensional perovskite quantum dots, where efficient defect passivation from the surface ligands and strong charge confinement in the nanocrystals has enabled photoluminescence quantum yields very close to unity.[25]

Another key aspect of any sensing material should be its stability under humid or ambient conditions. Degradation under atmosphere is a common problem with most organic and hybrid semiconductors, but recent research has shown that this issue is improving in hybrid perovskites.[29,30] Our own previous experiments with perovskite light emitters have shown that, while iodide-based perovskites degrade rapidly on contact with air, bromide-based perovskites tend to have surprisingly good stability even under ambient conditions without encapsulation. We have shown that perovskite lasers can operate in air with no observable degradation and still work well after many months of shelf storage.[31] It should also be noted that cesium-based perovskites are also known to be much more stable than their organic-based counterparts,[32] with some reports showing that $CsPbBr_3$ can even be immersed in water without degradation.[33,34] Whether this applies to films optimized for sensing, which by design are easily permeable to air and other potential sources of degradation, is not immediately clear. But it does show that there is strong potential for highly stable sensors in the future.

We aim to explore how these developments in tuning dimensionality to make light-emitting perovskites affect the sensing properties of hybrid perovskite films and use these insights to develop the next generation of light-emitting sensor materials. To explore the effect of dimensionality, we fabricated cesium lead bromide-based perovskite thin films with 3D, 2D, and 0D dimensionality using bulk $CsPbBr_3$, layered phenethylammonium $(PEA)_2Cs_2Pb_3Br_{10}$, and $CsPbBr_3$ nanocrystals, respectively. We then tested their quenching sensitivity to different explosive vapors compared to a pure nitrogen atmosphere to assess how the dimensionality affected their explosive sensing properties.

EXPERIMENTAL

In order to preserve consistency between experiments, all three dimensionalities were studied using perovskites with the same base components of cesium, lead, and bromine and were tested under identical conditions. To make the 3D perovskite films, cesium bromide (Sigma-Aldrich) and lead bromide (TCI, perovskite grade) were weighed out in a 1.05:1M ratio and then dissolved in dimethyl sulfoxide (DMSO) (Sigma-Aldrich, HPLC grade) with overnight stirring at 85 °C to make a 0.4M solution. Films were then produced by spin-coating the cooled solution at 8000 RPM onto precleaned glass substrates in a nitrogen-filled glovebox for 60 s, followed by annealing at 100 °C for 10 min. This resulted in films with roughly 100 nm thickness as measured by surface profilometry (Veeco Dektak 300).

For the 2D perovskite films, a 0.6M precursor solution was prepared by dissolving 220 mg $PbBr_2$, 81 mg phenethylammonium (PEA) bromide (Greatcell Solar), and 84 mg CsBr in 1 ml DMSO with overnight stirring at 85 °C. This composition was tuned to make a film of $(PEA)_2Cs_2Pb_3Br_{10}$, which has n = 3 stoichiometry. The cooled solution was then spin-coated at 3000 RPM onto a glass substrate for 90 s. At roughly 30 s into the spinning process, an antisolvent made from 300 μl of chloroform was rapidly dropped onto the film to encourage crystallization, and the final films were annealed at 100 °C for 10 min. To provide a comparison between organic- and inorganic-based films, another solution was made using 45 mg of methylammonium bromide (MABr) in place of the CsBr. It is important to note that the film quality is extremely sensitive to the timing of the chloroform wash step, and every batch of samples required some optimization beforehand to ensure that good quality films could be achieved. The resulting films were measured via surface profilometry to be roughly 150 nm thick.

The 0D perovskite nanocrystals were fabricated following previously reported procedures.[25] Cs_2CO_3 (0.814 g, 99.9%, Sigma-Aldrich) was loaded into 100 ml three-neck flask along with octadecene (ODE, 30 ml, 90%, Sigma-Aldrich) and oleic acid (2.5 ml, OA, 90%, Sigma-Aldrich), and the mixture was dried for 2 h at 120 °C under nitrogen. The solution temperature was then lowered to 100 °C. ODE (75 ml), oleylamine (7.5 ml, OLA, 90%, Sigma-Aldrich), dried OA (7.5 ml), and $PbBr_2$ (1.035 g, 99.999%, Sigma-Aldrich) were loaded into a 250 ml three-neck flask and dried under vacuum for 2 h at 120 °C. After complete solubilization of the $PbBr_2$ salt, the temperature was raised to 170 °C and the Cs-oleate solution (6.0 ml, 0.125M in ODE, prepared as described above) was quickly injected. After 10 s, the reaction mixture was cooled in an ice water bath. The nanocrystals were transferred to an argon glovebox (H_2O and O_2 < 1 ppm) precipitated from solution by the addition of equal volume anhydrous butanol (BuOH, 99%) (ODE:BuOH = 1:1 by volume). After centrifugation, the supernatant was discarded and the nanocrystals were redispersed in anhydrous hexane (99%) and precipitated again with the addition of BuOH (hexane:BuOH = 1:1 by volume). Finally, they were then dispersed in hexane to a concentration of 50 mg/ml^{-1}. This synthesis method produced cubic nanocrystals with an average size of 10.9 nm ± 0.5 nm as measured by transmission electron microscopy (shown in supplementary material). Given that the Bohr radius of excitons in halide perovskites is 2 nm–5 nm,[35] this is on the edge of what would be considered the quantum confinement regime (where the particle size is less than or equal to twice the Bohr radius). Nanocrystals of this nature are commonly referred to as "0D" in the literature,[36,37] and so given these conditions, we conclude that it is reasonable to use the 0D terminology. To obtain nanocrystal films, the solution was spin-coated onto cleaned glass substrates at 1500 RPM and dried at 90 °C for 5 min. The resulting films were of good quality, but were extremely fragile due to the poor self-adhesion of the nanocrystals. Hence, the sample thickness could not be measured via surface profilometry, and instead, the thickness of the films was measured to be 150 nm using angled scanning electron microscopy of a trench formed using a focused ion beam.

PETN, 2,4-dinitrotoluene (DNT), and RDX were obtained from Sigma-Aldrich, and TNT was obtained from XM-Materials. Fluorescence quenching experiments were carried out by placing the samples in a sealed chamber with a 10 l min^{-1} flow of nitrogen gas into which various analyte vapors could be introduced. The samples were excited by a 405 nm continuous-wave diode laser (Photonic Solutions) and the light emission monitored by a fiber-coupled Andor CCD spectrometer. Analyte vapors were introduced to the nitrogen flow via a vapor generator rig, which could direct the nitrogen flow through Pyrex Tubes containing ~1 g of analyte powder. The vapor passes through a cotton wool filter before entering the measurement chamber. Each sample was exposed to 30 s of clean nitrogen and then 195 s of analyte vapor, which was followed by 75 s of clean nitrogen vapor. Throughout the exposure, the photoluminescence of the samples was monitored. The timings were chosen to allow for the photostability of the sample to be evaluated and allow sufficient time for the analyte to interact with the film. The final exposure to clean nitrogen was used to investigate the reusability of the sensor. An upper limit to the sensitivity of the device can be estimated from these results by making the pessimistic assumption that the carrier gas flow is loaded with the analyte vapor at its saturated vapor pressure (see Table I). In practice, the vapor concentration is diluted from this level by the constant nitrogen flow across the source, which means that the incoming concentration of analyte is likely not saturated. This means that the sensitivity of the material calculated by assuming saturated conditions represents a lower bound. Absorption measurements were taken using a Varian Cary 300 absorption spectrometer, and fluorescence emission spectra were collected using an Edinburgh Instruments FLS980 fluorimeter. The ionization potential of 3D $CsPbBr_3$ was determined by ambient photoemission spectroscopy using a KP Technology APS-03 system.

RESULTS AND DISCUSSION

PL spectra

The absorption and PL spectra of all three dimensionalities of $CsPbBr_3$ perovskites are shown in Fig. 1. It can be seen that each material has a broad absorption band, increasing in strength at shorter wavelengths. The nanocrystal film has much weaker absorbance for a similar thickness because a large proportion of the film volume is made up of the spacer ligands, which do not contribute to the absorption, while the whole volume of the bulk film can contribute to absorption. Note that the 2D perovskite film shows a slow rise in absorption at the band edge, as opposed to the sudden onset seen in the other films. This is because the 2D film is made

TABLE I. Various explosive molecules, their HOMO and LUMO levels, and their saturated vapor pressures.

Explosive/material	HOMO level (eV)	LUMO level (eV)	Vapor pressure (ppb)	Molecular structure
DNT	−7.8	−3.2	180	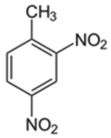
TNT	−8.5	−3.5	11	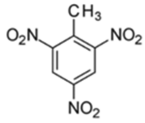
RDX	−8.2	−2.5	5×10^{-3}	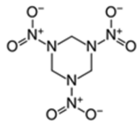
PETN	−6.8	−3.3	1.1×10^{-2}	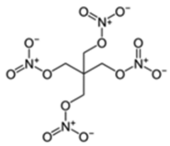
$CsPbBr_3$	−5.4	−3.1	N/A	N/A

up of many layers of the metal-halide octahedra separated by the phenethylammonium spacer ions. Each layer is an integer number of octahedra thick (denoted by their "*n* number"). The modal number of layers is tuned by the composition to be $n = 3$, but a broad distribution of many different *n* numbers are present, creating a stochastic mix of 2D quantum wells of varying width, with the low *n* wells having much wider bandgap and the high *n* wells approaching the bandgap of the bulk film. Hence, the density of states near the band edge is much lower than in the pure 3D case, since only the high *n* layers will absorb. A clear step at 425 nm can also be seen in the absorption spectrum, which corresponds to the bandgap of the $n = 1$ layer.

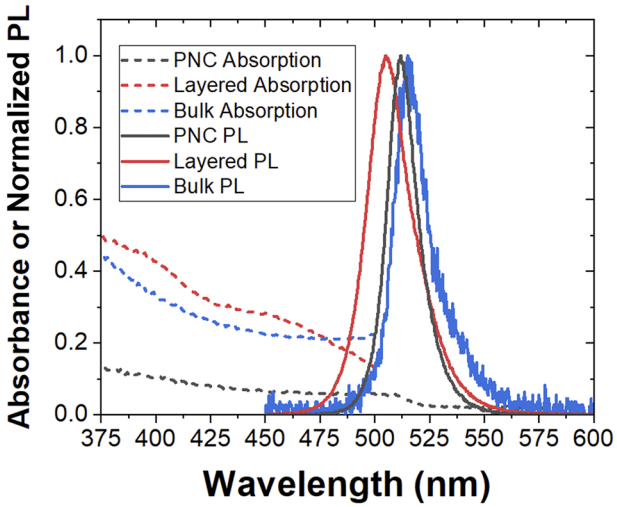

FIG. 1. PL (solid) and absorbance (dashed) spectra of cesium-based perovskite films. Blue shows bulk $CsPbBr_3$, blue shows $CsPbBr_3$ nanocrystal film, and red shows a film of quasi-2D $(PEA)_2Cs_2Pb_3Br_{10}$.

The structure of these films can also be clearly seen to affect the PL spectra. The nanocrystals have narrow PL, which is much stronger and blue-shifted compared to the bulk film. This blue shift comprises both a small shift in the high-energy edge, which we ascribe to weak quantum confinement, and the loss of the low energy tail in the PL, which is the more significant effect. We interpret the latter as indicating that the ligands in the nanocrystal films are effective in passivating surface defects in the perovskite nanocrystals, thus improving the photoluminescence quantum yield (PLQY) and removing emission from sub-bandgap states. The weak confinement is due to the relatively large size of these nanocrystals (cubes of 12 nm average side length), which means that their energy levels experience only a minor shift due to confinement effects. The 2D film also has strong PL and has its long-wavelength cutoff in the same place as the nanocrystals, which also indicates good passivation of surface defects. However, the overall PL spectrum extends much further into the blue than the other films, indicating that excitons in wide bandgap states are not all funneled into the lowest energy sites before emitting, leading to significant PL from layers with a lower

n number (and hence higher energy) than the bulk $CsPbBr_3$ crystal structure.

Surface morphology

To study how the analyte may interact with the films, we studied the surface morphology of the materials using scanning electron microscopy. As shown in Fig. 2(a), bulk $CsPbBr_3$ films exhibit polycrystalline morphology with characteristic features with micrometer length scales, while $(PEA)_2(Cs)_2Pb_3Br_{10}$ shows no discernible topography (measured using SEM). A nanocrystal film is shown in Fig. 2(b) and appears to have an amorphous, sponge-like morphology with myriad small cracks. The scanning electron microscope is not able to resolve the individual nanocrystals in this film, but studies with a transmission electron microscope show that this morphology itself consists of smaller grains ~11 nm across as shown in Figs. 2(c) and 2(d).

From these results, we can conclude that the nanocrystal films will have a very high effective surface area due to their spongy nature and small crystallite size, while the bulk films can be expected to get good quenching at the crystal boundaries, but the analytes are unlikely to be able to penetrate deep into the crystals. This could result in a weak response for the bulk film because it is common for most of the PL quenching in bulk perovskite films to occur at trap states at the crystal boundaries, so the introduction of an analyte may only act as a small modification to a site, which already has a high density of other quenchers. For the quasi-2D films , the PL response will depend on how easily the analyte can diffuse into the film, which is likely made of a very dense array of crystal domains that are smaller than the imaging resolution (several tens of nanometers) of the SEM.

Vapor sensing

As described above, for vapor sensing measurements with each sample, a reference PL measurement was performed under a flow of pure nitrogen, and the same sample was then measured with DNT gas flow in the same chamber. In Figs. 3–6 below, the gray areas represent the time that the vapor flow was turned on, and the white areas indicate periods of clean nitrogen flow. Figure 3 shows the PL response curves of 3D bulk $CsPbBr_3$ films exposed to either pure nitrogen or nitrogen with DNT vapors. It is shown in the figure that the response both under nitrogen and to DNT is very inconsistent. In two of the three samples, the PL drops by 20%–30% compared to the reference test over the course of a 3-min exposure. However, one of the samples shows no measurable change compared to the reference, and all three samples show substantially different reference curves. No recovery of the PL efficiency is observed in any of the samples after the vapor flow is turned off. This variability in stability,

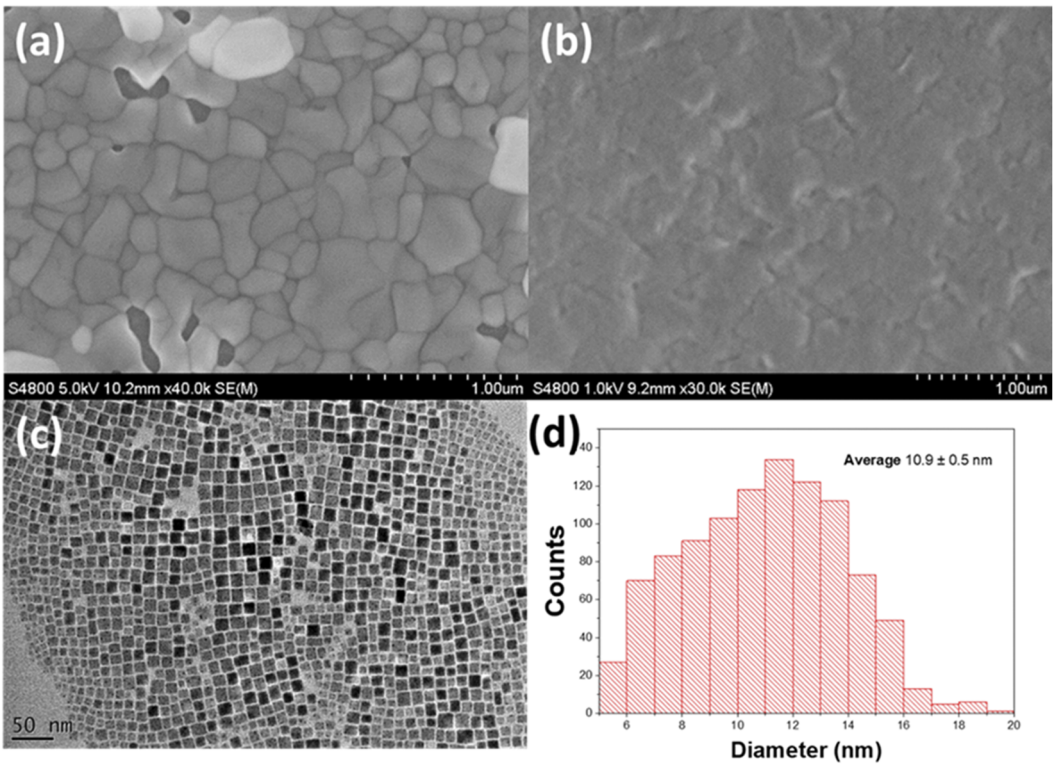

FIG. 2. Scanning electron microscopy images of (a) a bulk $CsPbBr_3$ film and (b) a $CsPbBr_3$ nanocrystal film. (c) Transmission electron microscopy image of the same kinds of nanocrystals to provide an estimate of crystallite size and shape, and the size distribution analysis is shown in (d).

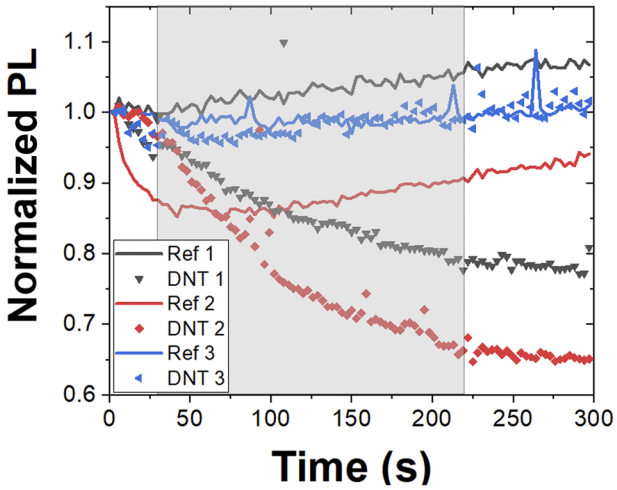

FIG. 3. PL response curves for three sample films of 3D $CsPbBr_3$ to gas flows of nitrogen (lines) and DNT vapor (symbols). Different colors represent the same test on different samples. The gray area, starting at 30 s and finishing at 225 s, denotes the period when the nitrogen was redirected through the reference tube or the tube containing the DNT. The white area denotes pure nitrogen flow.

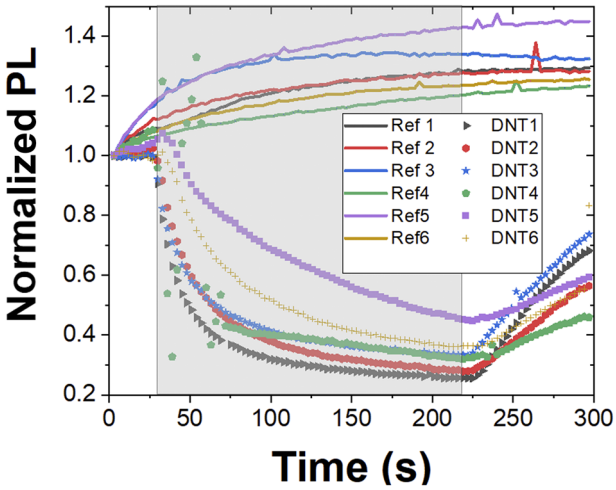

FIG. 5. PL response curves for three sample films of $CsPbBr_3$ nanocrystals to gas flows of nitrogen (lines) and DNT vapor (symbols). Different colors represent the same test on different samples. The gray area, starting at 30 s and finishing at 225 s, denotes the period when the nitrogen was redirected through the reference tube or the tube containing the DNT. The white area denotes pure nitrogen flow.

combined with the relatively weak and unreliable response, would make it very difficult to use in a real testing environment.

The inconsistent response to DNT vapors may be due to the 3D perovskite film having a low effective surface area due to its poor permeability, and the surfaces that are available for quenching already have a high (and potentially variable) density of quenching sites due to surface defects. We hypothesize that the poor sample-to-sample reproducibility is due to variations in the film morphology arising from the fabrication process. Depositing perovskite films from precursors is known to produce films with highly variable polycrystalline morphologies,[38] and a sample with many cracks present would have a much higher surface area for surface quenching of the PL than a more densely packed film. Hence, typical sample-to-sample variations of morphology may lead to the sample-to-sample variations in PL quenching in Fig. 3. The lack of reversibility in the measurement is also of interest, as it shows that the quenching is not simply a result of temporary adsorption of the

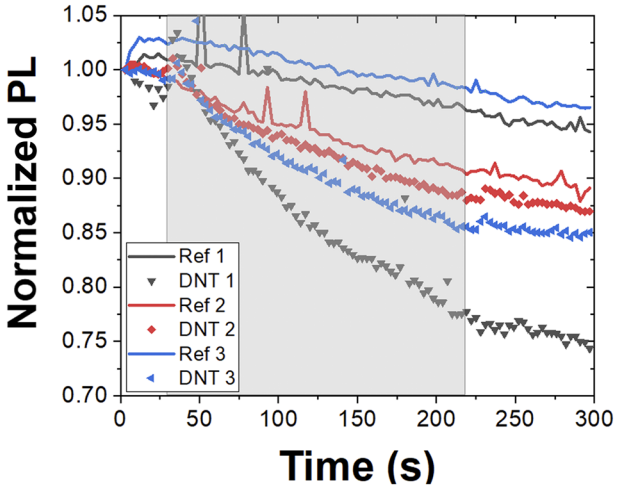

FIG. 4. PL response curves for three sample films of layered perovskite to gas flows of nitrogen (lines) and DNT vapor (symbols). Different colors represent the same test on different samples. The gray area, starting at 30 s and finishing at 225 s, denotes the period when the nitrogen was redirected through the reference tube or the tube containing the DNT. The white area denotes pure nitrogen flow.

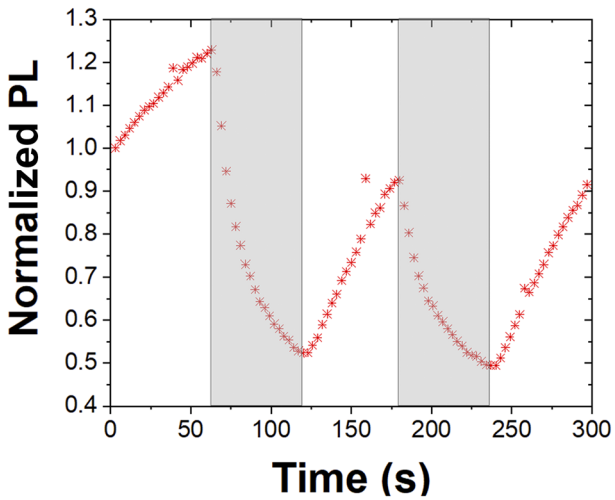

FIG. 6. PL vs time for a $CsPbBr_3$ nanocrystal film under repeated cycles of exposure to pure nitrogen (white areas) and DNT vapors in nitrogen (gray areas at 60-120 s and 180-240 s). It can be clearly seen that the PL rapidly decays when under DNT vapors, but it recovers when under pure nitrogen flow.

analyte and that the analyte is either permanently binding to the film, or possibly even acting as a catalyst for permanent degradation of the perovskite.

As discussed earlier, by introducing the phenethylammonium cation into the crystal structure, the bulk 3D film is split into layers of 2D quantum wells, which have a size-dependent bandgap and a much stronger exciton binding energy. The effect of this was clearly seen in the PL and absorption spectra, and it also significantly changes the behavior of the material in the sensing setup (as shown in Fig. 4). Firstly, while the baseline PL is much stronger than the 3D films, the samples show clear and consistent evidence of photodegradation under the control flow conditions where no DNT is present. The PL intensity of the samples reduces by between 5% and 10% over 3 min of testing, which will have to be accounted for when assessing the response to DNT.

Upon exposure to DNT, the samples do show increased quenching, with a more pronounced change in the slope of the PL decay following the start of the DNT vapor flow, although the strength of this change varies significantly from sample to sample. In one sample, the signal decays only slightly faster than the baseline with no DNT, while others show a 25% reduction over 3 min in DNT compared to a 3% decay under control conditions. There is no significant recovery in the PL efficiency after the DNT vapor flow is stopped. These results show some improvement over the 3D samples, with a clearer and more reproducible initial drop in PL intensity following the start of the DNT vapor flow.

While reducing the dimensionality in a perovskite film can potentially improve their sensing capability, the results are still inferior to those obtained from readily available organic semiconductors. We next further reduced the perovskite dimensionality by making films of perovskite nanocrystals (PNCs). The PNC films were found to have a PLQY comparable to that of the best 2D perovskite films and also showed much more consistent film quality because they were deposited from dispersion instead of from precursors.

Figure 5 shows the results of sensing tests with the PNC films. During the initial 3-min PL measurement under a clean nitrogen flow, the PNC films showed an increase in the PL intensity by up to 40%. This PL increase was consistently found to occur during the first few minutes of exposure to the 405 nm excitation laser, after which the PL efficiency was observed to stabilize. We found that this pre-exposure stabilization only occurred when the sample was illuminated, and not under nitrogen flow in the dark. We speculate that the increase may be due to photoinduced structural reorganization of the film.[39–41] The pre-exposure step gave a stable background against which to observe subsequent changes to the PL under exposure to DNT vapor. Upon subsequent exposure to DNT, the PNC films all showed a rapid drop in PL of up to 70% in 3 min, with most of the decay occurring in the first 60 s. This strong response means that a very large contrast between test and reference conditions was observed. Given that the concentration of DNT in the carrier gas will be no higher than the DNT saturated vapor pressure of 180 parts per billion, this demonstrates that the PNC films can have a strong response in at least the ppb range, and potentially lower. In addition to the significant decay upon exposure to DNT, a recovery of the PL is observed after the DNT flow is turned off, indicating that this quenching process is reversible and could be used to make reusable sensors.

To explore the reversibility of the PNC response to the DNT vapors, we performed a further experiment on the PNC films in which the DNT flow was cycled on and off for periods of 60 s at a time. The results are shown in Fig. 6, and the PL can be clearly seen to drop dramatically as soon as the vapor is turned on, and then recovers by ~50% of the initial drop over the 60 s when the DNT vapor is turned off. Further cycling of the DNT flows shows the PL decaying and recovering to approximately the same level each time, indicating that this is a consistent and reversible process. This shows that the adsorbed DNT molecules are only weakly attached and can readily desorb from the PNC surface. The difference in reversibility between the PNCs and other perovskite films may be attributed to the ligands attached to the PNCs (but not present in the other films), which could impede strong binding of the analyte to the optically active perovskite. The ligands attached to perovskite nanocrystals are known to be extremely dynamic and labile,[42] meaning that ligands can easily move aside to allow an incoming analyte access to the core, but could also rearrange back to their original state when the analyte diffuses away. When the DNT vapor is removed, the concentration gradient of the analyte is reversed, and so the weakly bound analyte molecules can easily desorb and diffuse away from the PNC film to reach a new equilibrium concentration with the clean carrier gas. These results are indicative of good repeatability, though a more detailed investigation into long-term repeatability and stability would be required to confirm this.

We consider this large, fast, and consistent quenching response to be due to several factors. First, the PNC films are far less dense than their 2D and 3D counterparts, with spacer ligands keeping the PNC cores from touching. This will provide easy pathways for the DNT to percolate into the film and will also give a much larger surface area for the reaction to occur. Hence, the response will be larger and faster. A similar enhancement of response time was previously seen by introducing porosity into a polymer used for explosive vapor sensing.[43] It should be noted that the presence of the ligands would be expected to slow down the quenching response somewhat, but this reduction in quenching rate is likely to be more than offset by the high surface-area-to-volume ratio of the nanocrystals. Additionally, the surface ligands on the PNCs passivate the existing traps on the surface of the perovskite crystals, and so quenching from the explosive analyte will have less competition from a native surface quenching process than the 2D and 3D perovskites. The weak and inconsistent response from the 2D films could also be partially due to the extremely hydrophobic nature of the PEA spacer ions in the crystal lattice, which may act to protect the light-emitting perovskite cores from interaction with the analyte and hence reduce the quenching effect. Finally, the improved consistency is likely due to the more consistent nature of depositing nanocrystals from solution as opposed to growing them from precursors *in situ* during spin coating, meaning that the effective area for reaction is less variable between samples.

Having established the most promising sensing response for DNT to be achievable using nanocrystalline perovskite, we assess its response to a selection of other target explosive molecules. An ideal targeted sensor would only respond to one kind of molecule, while a general sensor will respond to a wide range of molecules within a certain class. To test this, we repeated the PL sensing experiments with a range of other explosive molecules, including TNT, RDX, and PETN. The literature data for the chemical structures, vapor

pressures, and energy levels (taken by cyclic voltammetry) for each of these molecules are displayed in Table I.[44,45] We used the ionization potential of 3D $CsPbBr_3$, by ambient photoemission spectroscopy as an estimate of the HOMO energy, and then estimated the LUMO by adding the energy gap taken from the onset of the absorption spectrum (2.3 eV) to this value. As discussed in the section studying the PL, we expect the energy levels of our PNCs to be close to these bulk values because their relatively large size compared to other quantum dots means that the confinement effect will provide only small modifications to the energy levels. The magnitude of the sensing response, following a 3-min exposure to vapors of each explosive, is displayed in Fig. 7, and the full response curves for each other explosive are shown in the supplementary material. It can be seen that the PNC films have no significant response to TNT and PETN, and note that the slight increase in PL when exposed to RDX is likely not significant compared with a gradual increase in the PNC PL baseline.

TNT has a saturated vapor pressure of around 11 ppb, ~6% of that of DNT (180 ppb),[46,47] which appears to be consistent with the lower response observed for TNT. With conjugated polymer sensors, however, studies have found that TNT can cause roughly 25%–50% of the total quenching of DNT over a 5-min test.[48] This enhanced response to TNT compared with the relative vapor pressure can arise from differences in polymer-analyte binding properties in the film or the efficiency of electron transfer,[49,50] but these do not appear to be significant for the PNC sensors. In practical applications, the distinction between DNT and TNT is not very important, as any real-world TNT sample is contaminated by DNT from either production or degradation, and DNT is a significant component of the vapor plume emitted by a landmine.[51] The insignificant response to RDX and PETN may be due to their much lower vapor pressures (5 ppt and 11 ppt, respectively). Hence, there may be insufficient molecules accumulated from the vapor to cause a measurable change in the perovskite PL, at least over the same time scale as DNT detection. In addition, the shallow LUMO of RDX means that it would not be expected to quench.

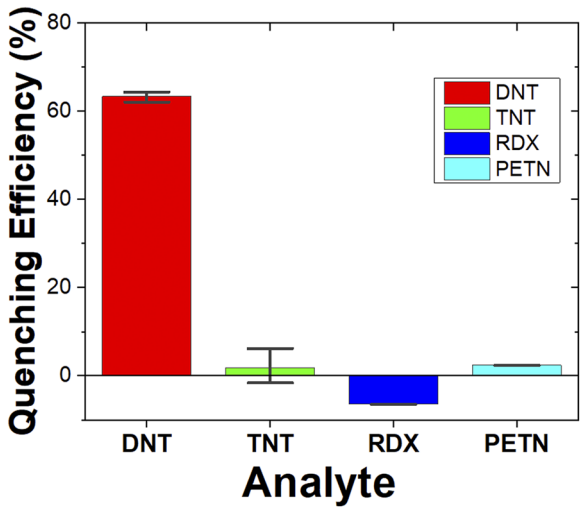

FIG. 7. The % drop in PL intensity of $CsPbBr_3$ nanocrystal films after 3 min of exposure to various explosive vapors when compared to control measurements under pure nitrogen.

CONCLUSIONS

In conclusion, we have shown that while 3D perovskite films show only a weak sensing response to explosive vapors, by tuning perovskite dimensionality, we can dramatically enhance the response of the films to external stimuli. In particular, we have shown how the low dimensionality and high surface area of perovskite nanocrystals lead to efficient PL quenching by DNT vapors. Our results suggest that $CsPbBr_3$ nanocrystal films can act as excellent sensors for a common vapor seen in landmines. The perovskite nanocrystal-based sensors show a quenching response of 70% over 3 min of exposure to DNT vapor in the parts per billion regime, and recovers by 50% of the initial value in 1 min once the analyte is removed. This demonstrates the great potential of perovskite nanocrystals as reusable sensors for explosive vapors.

AUTHORS' CONTRIBUTIONS

J.R.H. and J.M.E.G. contributed equally to the work.

SUPPLEMENTARY MATERIAL

See the supplementary material for the response curves of the nanocrystal films to RDX, TNT, and PETN.

ACKNOWLEDGMENTS

This project has received funding from the Engineering and Physical Sciences Research Council under Grant Nos. EP/T01119X/1 and EP/K503940/1, and the NATO Science for Peace and Security program under Grant No. MYP G5355. We would like to thank Dr. Lethy Krishnan Jagadamma for her help with scanning electron microscopy.

DATA AVAILABILITY

The data that support the findings of this study are openly available in the University of St Andrews Repository at https://doi.org/10.17630/934932a2-c721-4aff-9185-fc647ac20757.[52]

REFERENCES

[1]T.-H. Ong, T. Mendum, G. Geurtsen, J. Kelley, A. Ostrinskaya, and R. Kunz, "Use of mass spectrometric vapor analysis to improve canine explosive detection efficiency," Anal. Chem. **89**(12), 6482–6490 (2017).
[2]L. Lit, J. B. Schweitzer, and A. M. Oberbauer, "Handler beliefs affect scent detection dog outcomes," Animal Cognit. **14**(3), 387–394 (2011).
[3]T. M. Swager, "The molecular wire approach to sensory signal amplification," Acc. Chem. Res. **31**(5), 201–207 (1998).
[4]S. Rochat and T. M. Swager, "Conjugated amplifying polymers for optical sensing applications," ACS Appl. Mater. Interfaces **5**(11), 4488–4502 (2013).

[5]S. W. Thomas III, J. P. Amara, R. E. Bjork, and T. M. Swager, "Amplifying fluorescent polymer sensors for the explosives taggant 2,3-dimethyl-2,3-dinitrobutane (DMNB)," Chem. Commun. **2005**(36), 4572–4574.
[6]T. M. Swager and J. H. Wosnick, "Self-amplifying semiconducting polymers for chemical sensors," MRS Bull. **27**(6), 446–450 (2002).
[7]S. J. Toal and W. C. Trogler, "Polymer sensors for nitroaromatic explosives detection," J. Mater. Chem. **16**(28), 2871–2883 (2006).
[8]E. Rugged, Handheld Explosives Trace Detector, 2020, available from https://www.flir.co.uk/products/fido-x3/; 14 April 2020.
[9]A. Arbense, Next-Generation Explosive Detection, 2020, available from http://www.arborescent.com/; 14 April 2020.
[10]R. N. Gillanders, I. D. W. Samuel, and G. A. Turnbull, "A low-cost, portable optical explosive-vapour sensor," Sens. Actuators, B **245**, 334–340 (2017).
[11]Q. Wali *et al.*, "Advances in stable and flexible perovskite solar cells," Curr. Appl. Phys. **20**(5), 720–737 (2020).
[12]Y. Zou, Z. Yuan, S. Bai, F. Gao, and B. Sun, "Recent progress toward perovskite light-emitting diodes with enhanced spectral and operational stability," Mater. Today Nano **5**, 100028 (2019).
[13]Y. Ouyang *et al.*, "Photo-oxidative degradation of methylammonium lead Iodide perovskite: Mechanism and protection," J. Mater. Chem. A **7**, 2275 (2018).
[14]H. Wei and J. Huang, "Halide lead perovskites for ionizing radiation detection," Nat. Commun. **10**(1), 1066 (2019).
[15]M. A. Haque *et al.*, "Giant humidity effect on hybrid halide perovskite microstripes: Reversibility and sensing mechanism," ACS Appl. Mater. Interfaces **11**(33), 29821–29829 (2019).
[16]K. Xia *et al.*, "CVD growth of perovskite/graphene films for high-performance flexible image sensor," Sci. Bull. **65**(5), 343–349 (2020).
[17]J. Miao and F. Zhang, "Recent progress on highly sensitive perovskite photodetectors," J. Mater. Chem. C **7**(7), 1741–1791 (2019).
[18]H.-H. Fang *et al.*, "Ultrahigh sensitivity of methylammonium lead tribromide perovskite single crystals to environmental gases," Sci. Adv. **2**(7), e1600534 (2016).
[19]S. Ruan *et al.*, "An optical fibre-based sensor for the detection of gaseous ammonia with methylammonium lead halide perovskite," J. Mater. Chem. C **6**(26), 6988–6995 (2018).
[20]M.-Y. Zhu *et al.*, "A fluorescence quenching sensor for Fe^{3+} detection using $(C_6H_5NH_3)_2Pb_3I_8{\cdot}2H_2O$ hybrid perovskite," Inorg. Chem. Commun. **109**, 107562 (2019).
[21]C. Muthu, S. R. Nagamma, and V. C. Nair, "Luminescent hybrid perovskite nanoparticles as a new platform for selective detection of 2,4,6-trinitrophenol," RSC Adv. **4**(99), 55908–55911 (2014).
[22]N. Wang *et al.*, "Perovskite light-emitting diodes based on solution-processed self-organized multiple quantum wells," Nat. Photonics **10**(11), 699–704 (2016).
[23]Y. Sun *et al.*, "The formation of perovskite multiple quantum well structures for high performance light-emitting diodes," npj Flexible Electron. **2**(1), 12 (2018).
[24]X. Zhang *et al.*, "Controlled synthesis and photonics applications of metal halide perovskite nanowires," Small Methods **3**(1), 1800294 (2019).
[25]F. Zhang *et al.*, "Brightly luminescent and color-tunable colloidal $CH_3NH_3PbX_3$ (X = Br, I, Cl) quantum dots: Potential alternatives for display technology," ACS Nano **9**(4), 4533–4542 (2015).
[26]H. H. Fang *et al.*, "Band-edge exciton fine structure and exciton recombination dynamics in single crystals of layered hybrid perovskites," Adv. Funct. Mater. **30**(6), 1907979 (2020).
[27]Z.-K. Tan *et al.*, "Bright light-emitting diodes based on organometal halide perovskite," Nat. Nanotechnol. **9**(9), 687–692 (2014).
[28]K. Lin *et al.*, "Perovskite light-emitting diodes with external quantum efficiency exceeding 20 per cent," Nature **562**(7726), 245–248 (2018).
[29]I. Deretzis *et al.*, "Stability and degradation in hybrid perovskites: Is the glass half-empty or half-full?," J. Phys. Chem. Lett. **9**(11), 3000–3007 (2018).
[30]M. Liu *et al.*, "Improving the stability of $CsPbBr_3$ perovskite nanocrystals by peroxides post-treatment," Front. Mater. **6**, 306 (2019).
[31]J. R. Harwell *et al.*, "Green perovskite distributed feedback lasers," Sci. Rep. **7**(1), 011727 (2017).
[32]R. E. Beal *et al.*, "Cesium lead halide perovskites with improved stability for tandem solar cells," J. Phys. Chem. Lett. **7**(5), 746–751 (2016).
[33]G. Chen *et al.*, "Ultra-high stability of cesium lead halide nanocrystals synthesized by a simple one-pot method," Mater. Des. **181**, 108100 (2019).
[34]L. Gomez *et al.*, "Color-stable water-dispersed cesium lead halide perovskite nanocrystals," Nanoscale **9**, 631 (2017).
[35]A. S. Berestennikov *et al.*, "Beyond quantum confinement: Excitonic nonlocality in halide perovskite nanoparticles with mie resonances," Nanoscale **11**(14), 6747–6754 (2019).
[36]Y. Zhang *et al.*, "Zero-dimensional Cs_4PbBr_6 perovskite nanocrystals," J. Phys. Chem. Lett. **8**(5), 961–965 (2017).
[37]Y. Dong *et al.*, "Recent advances toward practical use of halide perovskite nanocrystals," J. Mater. Chem. A **6**(44), 21729–21746 (2018).
[38]M. A. Haque, J. Troughton, and D. Baran, "Processing-performance evolution of perovskite solar cells: From large grain polycrystalline films to single crystals," Adv. Energy Mater. **10**(13), 1902762 (2020).
[39]S. G. Motti *et al.*, "Photoinduced emissive trap states in lead halide perovskite semiconductors," ACS Energy Lett. **1**(4), 726–730 (2016).
[40]D. Parobek *et al.*, "Photoinduced anion exchange in cesium lead halide perovskite nanocrystals," J. Am. Chem. Soc. **139**(12), 4358–4361 (2017).
[41]R. Gottesman *et al.*, "Photoinduced reversible structural transformations in free-standing $CH_3NH_3PbI_3$ perovskite films," J. Phys. Chem. Lett. **6**(12), 2332–2338 (2015).
[42]J. De Roo *et al.*, "Highly dynamic ligand binding and light absorption coefficient of cesium lead bromide perovskite nanocrystals," ACS Nano **10**(2), 2071–2081 (2016).
[43]Y. Wang, N. B. McKeown, K. J. Msayib, G. A. Turnbull, and I. D. W. Samuel, "Laser chemosensor with rapid responsivity and inherent memory based on a polymer of intrinsic microporosity," Sensors **11**, 2478–2487 (2011).
[44]S. S. Nagarkar *et al.*, "Highly selective detection of nitro explosives by a luminescent metal–organic framework," Angew. Chem., Int. Ed. **52**(10), 2881–2885 (2013).
[45]R. Tsyshevsky *et al.*, "Photochemistry of the α-Al_2O_3-PETN interface," Molecules **21**(3), 289 (2016).
[46]R. G. Ewing *et al.*, "The vapor pressures of explosives," TrAC, Trends Anal. Chem. **42**, 35–48 (2013).
[47]H. Östmark, S. Wallin, and H. G. Ang, "Vapor pressure of explosives: A critical review," Propellants, Explos., Pyrotech. **37**(1), 12–23 (2012).
[48]J.-S. Yang and T. M. Swager, "Porous shape persistent fluorescent polymer films: An approach to TNT sensory materials," J. Am. Chem. Soc. **120**(21), 5321–5322 (1998).
[49]Y. Li *et al.*, "Coordination polymer nanoarchitecture for nitroaromatic sensing by static quenching mechanism," J. Phys. Chem. C **119**(51), 28544–28550 (2015).
[50]N. Bolse *et al.*, "A digitally printed optoelectronic nose for the selective trace detection of nitroaromatic explosive vapours using fluorescence quenching," Flexible Printed Electron. **2**(2), 024001 (2017).
[51]T. F. Jenkins *et al.*, "Chemical signatures of TNT-filled land mines," Talanta **54**(3), 501–513 (2001).
[52]J. R. Harwell, J. M. E. Glackin, N. J. L. K. Davis, R. N. Gillanders, D. Credgington, G. A. Turnbull, and I. D. W. Samuel, Sensing of Explosive Vapor by Hybrid Perovskites—Effect of Dimensionality (Dataset), University of St Andrews Data Repository, 2020, https://doi.org/10.17630/934932a2-c721-4aff-9185-fc647ac20757.